Numerical Analysis of Welding Residual Stress Using Heat Source Models for the Multi-Pass Weldment

Dong Ho Bae*
School of Mechanical Engineering, Sungkyunkwan University, Kyunggido 440-746, Korea
Chul Han Kim, Seon Young Cho
Mechanical Engineering Department, Sungkyunkwan University, Kyunggido 440-746, Korea
Jung Kyun Hong
Research Scientist, Battelle Memorial Institute, 505 King Avenue, Columbus, Ohio, USA Zip code; OH43201-2693
Chon Liang Tsai
Department of Industrial, Welding and Systems Engineering, The Ohio State University, 1250 Arthur E. Adams Drive, Columbus, Ohio, USA Zip code: OH 43221

Numerical prediction of welding-induced residual stresses using the finite element method has been a common practice in the development or refinement of welded product designs. Various researchers have studied several thermal models associated with the welding process. Among these thermal models, ramp heat input and double-ellipsoid moving source have been investigated. These heat-source models predict the temperature fields and history with or without accuracy. However, these models can predict the thermal characteristics of the welding process that influence the formation of the inherent plastic strains, which ultimately determines the final state of residual stresses in the weldment. The magnitude and distribution of residual stresses are compared. Although the two models predict similar magnitude of the longitudinal stress, the double-ellipsoid moving source model predicts wider tensile stress zones than the other one. And, both the ramp heating and moving source models predict the stress results in reasonable agreement with the experimental data.

Key Words : Heat Source Model, Numerical Analysis, Welding Residual Stress, Ramp Heat Input Model, Double-Ellipsoid Moving Heat Source Model, Longitudinal Residual Stress

1. Introduction

Welding is practically used in every industry and is associated with a very large part of the country's gross national product. Welding processes are vital in the production and maintenance of pipelines and power plants, in the areas of heavy construction, and in shipbuilding, machinery manufacturing, and every phase of activities associated with transportation. In addition, welding is used in such diverse areas as microcircuit fabrication and in the casting industry. In many key-manufacturing operations, the vital matter of productivity is directly tied to welding.

One common problem associated with welding, that has been realized and documented for many

* Corresponding Author,
E-mail : bae@yurim.skku.ac.kr
TEL : +82-31-290-7443; **FAX** : +82-31-295-1937
Professor, School of Mechanical Engineering, Sungkyunkwan University, 300, Chunchun-Dong, Jangan-Gu, Suwon, Kyungki-Do 440-746, Korea. (Manuscript **Received** August 27, 2001; **Revised** June 10, 2002)

years, is welding residual stress as well as distortion of the finished products. As a result of fusion welding process, high tensile residual stresses are generated near the weld metal and compressive residual stresses are formed in the base metal due to the large nonlinear thermal loading created by a moving heat source. The thickness of the plates in structures usually requires multi-pass welding processes. In this case, the non-linearity of thermal loading is more severe due to the multiple thermal cycles, which create more complex residual stress distributions than those in the single-pass welding process. These residual stresses add to the primary load stresses to increase the crack driving force and strain at the crack tip front that promotes premature brittle fracture of the welded joint. Accurate estimate of welding-induced residual stresses in the design stage could prevent costly mitigation requirements after completion of the welding process.

Many investigators have attempted to establish empirical approaches for understanding the thermal and mechanical behaviors of weldment. To date, however, due to complexity of the welding process, they are not completely understood. Considerable efforts have been devoted to develop analytical approaches to predict the thermal and mechanical responses of the weldments. Although, some insightful results have been obtained, they are difficult to implement in realistic welded structures due to severe limitations in the geometry of the weldments and the inherent assumption made to derive the equations. More effort has been therefore expanded to develop numerical models to predict the transient thermal and residual stress responses following the progress of computer technology. Subsequently, some numerical modeling technologies have been developed. One of the most powerful and widely used numerical analyses is the finite element method (FEM). The FEM can handle non-linear behaviors, such as complicated geometry, complex boundary conditions, and temperature dependant material properties.

There are many publications on weld modeling using FEM (Ueda, 1982; Feng, 1989; Goldak, 1990; Tsai, 1991; Shim, 1992; Hong, 1994; Dong, 1997; Hibbitt, 1973; Leung, 1990; Seok et al., 1999). Recently, additional efforts have also been made to develop simplified finite element analysis (FEA) procedures so that realistic temperature and stress histories in a weldment can be simulated with commonly available FEA packages. Representative publications on FEA techniques for the multi-pass welds can be found in many literatures (Feng, 1989; Tsai, 1991, 1992; Shim, 1992; Hong, 1994; Dong, 1997). The thermal and mechanical responses of a weldment are a three-dimensional problem that requires a considerable amount of computation time to simulate a multi-pass weld joint. This computation time increases in proportion to the number of weld passes and may make the FEM unrealistic to predict the residual stresses. It is therefore necessary to develop cost-effective, numerical procedures to reduce the computation time while still preserving the accuracy of the solution. To reduce the computation time, depending upon the nature of the problem (Tsai, 1991; Shim, 1992; Hong, 1994), a two-dimensional analysis can be carried out for a three-dimensional solution with appropriate simplifications.

To simulate the multi-pass effect, various element rebirth techniques have been used and incorporated in the existing commercial FEA packages. These element groups are kept inactive until a designated "rebirth" time, according to the specified pass sequence, is approached in the simulation. For each activated weld pass, various heat-input models have been investigated. Two commonly used source models with increasing degree of complexity are ramp heat input model (Model I) and double-ellipsoid moving source model (Model II). These heat-source models predict the temperature fields and history with or without accuracy, or even incorrect. However, they can predict the thermal characteristics of the welding process that influence the formation of the inherent plastic strains, which ultimately determines the final state of residual stresses in the weldment.

This paper investigates these two commonly used heat-source models in prediction of residual stresses in a multi-pass-welded plate. Experi-

mental results are also presented to validate the predictions. The magnitude and distribution of residual stresses are compared.

2. Welding Heat Source Models

2.1 Heat input model with ramp function

The heat-input model using the ramp function (Model I), of which concept is based on Pavelic's 'disc' model (Pavelic et al., 1969), was developed by Tsai *et al.* (1992). In the 'disc' model, this modified heat flux has a Gaussian or normal distribution in the plane.

$$q(x)=q(0)\,e^{-Ax^2} \tag{1}$$

Where $q(0)$ is the maximum heat flux at the center of the heating spot, A is the heat flux concentration coefficient.

The conservation of energy over the heat input surface may be written as

$$Q=q(0)\sqrt{\frac{\pi}{A}}L \tag{2}$$

L is the width of weld bead (unit : mm). For heat flow analysis of thick-section weld joint, a weld cross-section of unit length is used in lieu of the entire joint length. The analysis becomes a two-dimensional model. The effect of travel is incorporated in the ramp heat function of the arc scanning time (i.e. time required for an arc to scan across an unit weld length). It may be assumed that a distance from the arc center, b (unit : mm), where the heat flux drops to 5% of the maximum value, bound the effective heat input domain on the heat input surface. The heat flux concentration coefficient, A, can be obtained from this assumption and written as

$$q(b)=q(0)\,e^{-Ab^2}=0.05q(0) \tag{3}$$

where

$$A\cong\frac{3}{b^2} \tag{4}$$

Substituting A and $q(0)$ from Eqs. (2) and (4) into Eq. (1), the surface heat flux distribution function $q(x)$ can be obtained as

$$q(x)=\frac{Q}{bL}\sqrt{\frac{3}{\pi}}e^{-3\left(\frac{x}{b}\right)^2} \tag{5}$$

When a constant heat input is used in the thermal analysis, the total heat input applied to the weld consists of two parts : surface heat input and body heat input.

$$Q=Q_S+Q_B \tag{6}$$

Where Q_S and Q_B are surface and body heat inputs, respectively. The total linear heat input (i.e. energy per unit weld length) and the respective heat fluxes may be calculated using the following equations :

Heat input energy (J/mm): $H=Q\cdot\frac{1}{v}$ (7)

Body heat flux (W/mm^3): $q_B=\frac{Q_B}{V_e}$ (8)

Surface heat flux (W/mm^2):

$$q_S=\frac{Q_S}{bL}\sqrt{\frac{3}{\pi}}e^{-3\left(\frac{x}{b}\right)^2} \tag{9}$$

Where Q is net heat input from the arc, v is welding speed (mm/sec), V_e is the volume of bead elements in which body heat flux is applied (mm^3).

In the ramp heat input model, a ramp heating function is usually used to avoid numerical divergence problems due to an instantaneous increase in temperature near the fusion zone. It is also used to distribute the energy in arc scanning time domain to incorporate the fast heating and slower cooling phenomena, which is associated with any typical moving source problem.

A characteristic ramp heat function is graphically shown in Fig. 1. The arc scanning time over the unit weld length is $1/v=t_1+t_2$. Part of the total energy is moved from early scanning period, t_1, to later time, t_3, to incorporate the heat-

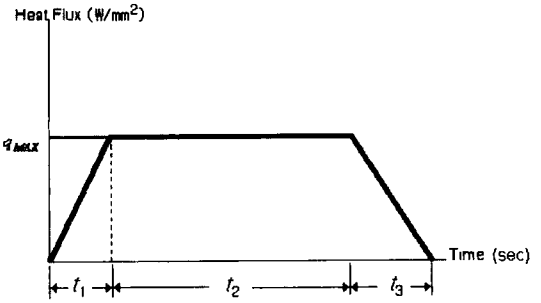

Fig. 1 Shape of ramp heat input function (Hong, 1996)

ing and cooling phenomena. The total heating energy over the $1/v$ scanning period should remain the same.

It has been reported that the temperature predictions using the ramp heat-input model is relatively insensitive to the ramp function. And, Shim et al. (1992) recommends a 20% of ramping time (i.e. $t_1/(t_1+t_2)$) for the optimum results.

2.2 Double ellipsoidal heat input model

The double ellipsoidal model (Model II), originally proposed by Goldak *et al.* (1984), is based on a double Gaussian power density distribution in the domains before and after the arc center. The Gaussian distributions of the power density in an ellipsoid with center at (0, 0, 0) and semi-axes a, b, c parallel to the moving coordinate axes x, y, ξ in Fig. 2 can be written as:

$$q(x, y, \xi)=q(0)\,e^{-Ax^2}e^{-By^2}e^{-C\xi^2} \tag{10}$$

where $q(0)$ is the maximum value of the power density at the center of the ellipsoid. Conservation of energy requires that:

$$2Q=2\eta VI =8\int_0^\infty\int_0^\infty\int_0^\infty q(0)\,e^{-Ax^2}e^{-By^2}e^{-C\xi^2}dxdyd\xi \tag{11}$$

Where: η=heat source efficiency, V=voltage, I=current

Evaluating Eq. (11) produces the following:

$$2Q=\frac{q(0)\,\pi\sqrt{\pi}}{\sqrt{ABC}} \tag{12}$$

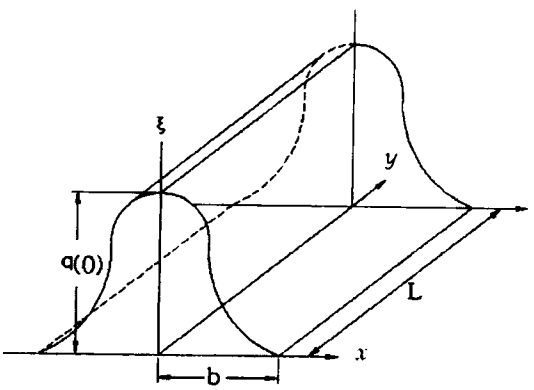

Fig. 2 Modified Gaussian heat input scheme (Hong, 1996)

$$q(0)=\frac{2Q\sqrt{ABC}}{\pi\sqrt{\pi}} \tag{13}$$

To evaluate the constants, A, B, C, the semi-axes of the ellipsoid a, b, c in their respective directions, x, y, ξ can be defined such that the power density falls to $0.05q(0)$ at the surface of the ellipsoid. Hence,

$$A\approx\frac{3}{a^2},\ B\approx\frac{3}{b^2},\ C\approx\frac{3}{c^2} \tag{14}$$

$q(0)$ is calculated by considering conservation of energy, which is $Q=\eta VI$. Therefore,

$$q(x, y, \xi)=\frac{6\sqrt{3}\,Q}{abc\pi\sqrt{\pi}}e^{-3x^2/a^2}e^{-3y^2/b2}e^{-3\xi^2/c^2} \tag{15}$$

In the mechanical analysis, it is sometimes convenient to introduce the global coordinate system (x, y, z), which is fixed in the workpiece. In addition, a lag factor τ is used to define the position of the heat source relative to the center of the heating ellipsoid. The transformation relating the fixed and moving coordinate systems is,

$$\xi=z+v(\tau-t) \tag{16}$$

where ξ=coordinate in the travel direction with its origin attached to the moving source, v= welding speed (mm/s), τ=lag factor and t= welding time.

The coordinate transformation can be substituted into Eq. (15) to provide an expression for the ellipsoid in the fixed coordinate system.

$$q(x, y, z, t)=\frac{6\sqrt{3}\,Q}{abc\pi\sqrt{\pi}}e^{-3\frac{x^2}{a^2}}e^{-3\frac{y^2}{b^2}}e^{\frac{-3[z+v(\tau-t)]^2}{c^2}} \tag{17}$$

If heat flow in the y direction is neglected, an analysis can be performed on the x-y plane located at y=0, which becomes the 'disc' source as proposed by Krutz and Segerlind (1978).

Calculations with the ellipsoidal heat source model have revealed that the temperature gradient in front of the heat source is not as step as expected and the gentler gradient at the trailing edge of the molten pool is steeper than experimental experience. To overcome this limitation, two ellipsoidal sources are combined as shown in Fig. 3. The front half of the source is the quadrant of one ellipsoidal source, and the rear half is the quadrant of another ellipsoid.

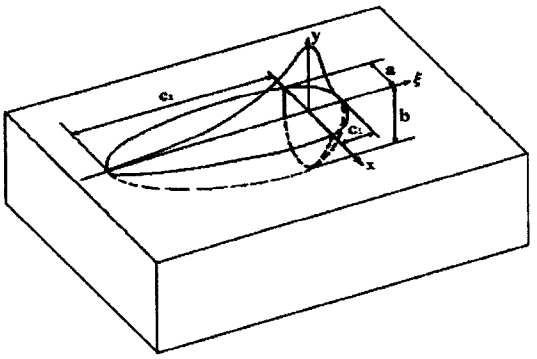

c_1, c_2 ; the semi axis c in the front and rear quadrant along the ξ axis of the double ellipsoidal heat source model

Fig. 3 Double ellipsoid heat source configuration (Goldak, 1984)

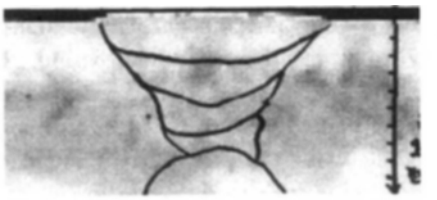

(a) Cross section of the welded specimen

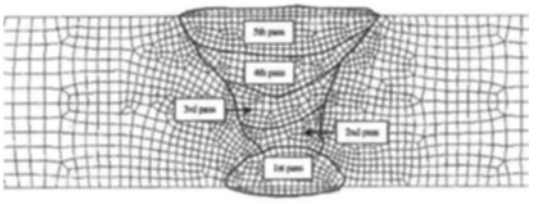

(b) Finite element mesh

Fig. 4 Cross section of the welded specimen and finite element mesh

The power density distributions along the ξ axis of the double ellipsoidal heat source model are shown in Fig. 3. In this model, the fractions f_f and f_r of the heat deposition in the front and rear quadrants are needed, where $f_f+f_r=2$. The power density distribution inside the front quadrant becomes :

$$q(x, y, z, t)=\frac{6\sqrt{3}f_fQ}{abc\pi\sqrt{\pi}}e^{-3\frac{x^2}{a^2}}e^{-3\frac{y^2}{b^2}}e^{\frac{-3[z+v(\tau-t)]^2}{c^2}} \quad (18)$$

Similarly, the power density distribution for the rear quadrant of the source inside the ellipsoid becomes :

$$q(x, y, z, t)=\frac{6\sqrt{3}f_rQ}{abc\pi\sqrt{\pi}}e^{-3\frac{x^2}{a^2}}e^{-3\frac{y^2}{b^2}}e^{\frac{-3[z+v(\tau-t)]^2}{c^2}} \quad (19)$$

3. Finite Element Analysis (FEA)

3.1 FEA Modeling

A five-pass welded plate model was considered in this study. The thickness was 10 mm and the width of the model was 200 mm. The width of the final weld pass was 12 mm. Two-dimensional finite element analysis models were used for both thermal and mechanical analyses using the respective heat source models. The cross-section of the actual test specimen and the finite element model are shown in Fig. 4(a) and (b), respectively.

In the finite element models, four-node heat transfer elements and six-node generalized plane strain elements were used. The area with oblique lines represents the layers of the weld bead determined by the actual weld coupon. Finer meshes were generated in the weld metal regions to handle the greater non-linearity and to obtain accurate results.

I-DEAS, a commercial pre-and post-processor was used for the mesh generation. ABAQUS was employed for the transient temperature and subsequent residual stress analyses. The total number of elements is 1944 and the total number of nodes is 2080.

The chemical composition and room temperature mechanical properties of the modeled material (i.e. SUS304L stainless steel) are shown in Tables 1 and 2, respectively. The gas tungsten arc welding (GTAW) process was used in the experiment and modeled in the finite element analysis. The welding conditions are given in Table 3. The temperature dependent material properties of SUS304L stainless steel are shown in Fig. 5 (a) and (b). Both the thermal conductivity and the specific heat increase linearly in the whole temperature range from room temperature to 1000 ℃. The elastic modulus and the yield strength decrease with increasing temperature. On the contrary, the thermal expansion coefficient increases linearly with temperature between room temperature and 1000 ℃.

Table 1 Chemical compositions of the specimen

SUS 304L		C	Si	Mn	P	S	Ni	Cr+Mo	Cu
	Base Metal	0.08	1.0	2.0	0.05	0.03	8	18	
GTAW	Weld Metal	0.03	0.7	2.5	0.03	0.03	9	21	0.8

Table 2 Mechanical properties of the specimen

	Tensile properties		
SUS 304L	Yield Strength MPa	Tensile Strength MPa	Elongation
	290	579	55%

Table 3 Welding conditions for a five-pass welded plate

Pass Number	welding Parameters		
	Current (Amp.)	Voltage (V)	Travel Speed (m/min)
1	90	14	0.09
2	120	16	0.11
3	120	16	0.11
4	120	16	0.11
5	120	16	0.11

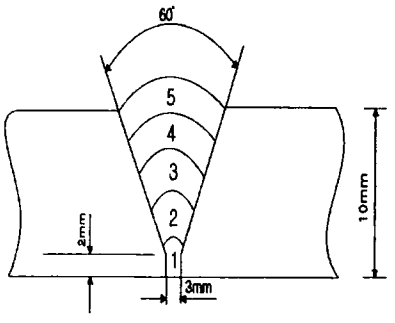

Electrode : ER308L

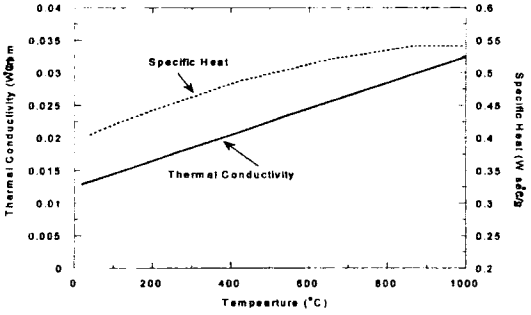

(a) Thermal properties

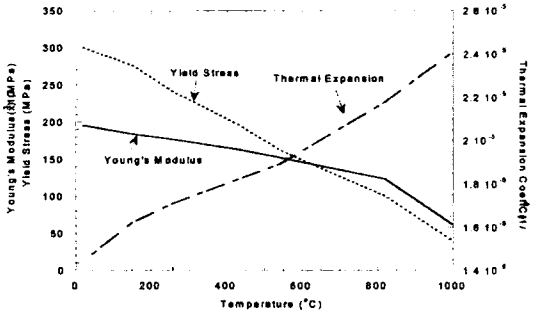

(b) Mechanical properties

Fig. 5 Temperature dependent material properties of 304L stainless steel

3.2 Analysis of temperature history and residual stress distribution

3.2.1 Assumptions and simulation procedures

Two welding simulations were performed under identical conditions except the heat source model. The uncoupled thermo-mechanical analysis was conducted, which means that the temperature fields and histories were calculated from the thermal analysis and then used as an input database for the subsequent stress analysis. Identical time steps were used for both thermal and mechanical analyses. The numerical procedures

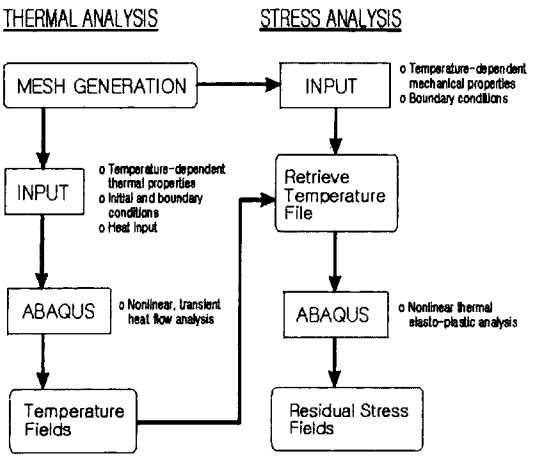

Fig. 6 Numerical procedures for an uncoupled thermo-mechanical analysis (Hong, 1996)

for the uncoupled thermo-mechanical analysis are shown in Fig. 6. In performing the temperature analysis, it was assumed that the initial temperatures of base and weld metals were assumed at a constant room temperature (21 ℃). The temperature dependent material properties were used in the analysis. However, the conductivity and specific heat in the molten pool were assumed to be constant. The effect of latent heat of fusion, which is the internal energy change during melting or solidification, was also considered in the thermal analysis.

The heat loss coefficient applied to all exposed surfaces was 0.0817W/m^2-℃ (0.0001 Btu/in^2-°F). Other thermal boundary conditions such as radiation and forced convection due to the shielding gas flow were neglected. These terms only become significant when the behavior of a molten pool flow is of interest. Because of the high temperatures in the molten pool, it is trivial in the residual stress simulations. Similarly, radiation and convection influences on the microstructures and cooling rates in weld metal, as well as heat losses or gains from phase transformation were neglected. The effect of radiation was incorporated in the thermal efficiency (η) and the volume change effect due to phase transformation was also neglected in the stress analysis.

In performing the stress analysis, the mechanical and physical properties of yield stress, elastic and plastic moduli, and thermal expansion coefficient were considered temperature dependent. Mechanical properties were however assumed constant above the melting point. The temperature dependency of Poisson's ratio was neglected. A constant value of 0.32 was used for SUS304L stainless steel in the analysis.

The element rebirth technique (Hong, 1994) was employed to include the multi-pass weld metal deposition effects. With this technique, the elements simulating each weld pass were grouped at the model generation stage. During analysis, these element groups which presented weld passes were first removed and then reactivated at a specified moment to simulate a given deposition sequence of weld passes. When a group of weld elements were activated, specific initial temperatures were imposed at all nodes associated with the weld elements.

The heat input was imposed onto the specific newly activated element groups representing a depositing pass at a given time according to the characteristics of the different heat source models, i.e., Model I and Model II. The heat input fractions for Model II were empirically determined as $f_f=0.6$ and $f_r=1.4$ (Goldak, 1984).

4. Results and Discussion

4.1 Transient temperature profiles

The temperature histories at a location 5 mm away from the weld toe of the final pass predicted using the heat-source models are shown in Fig. 7. The experimental data measured at the same location, which is acquired in this study, is compared with the numerically calculated results in the same figure. The predicted temperature history from numerical analyses shows good agreement with measured values during the weld heating cycle. The thermal models however underestimated the temperatures during the cooling cycle. The predicted temperatures from the two models are very close, with the moving source model predicting higher peak temperature.

As mentioned earlier in this paper, the temperature predictions are unrealistic. For the two heat-source models, the close resemblance in

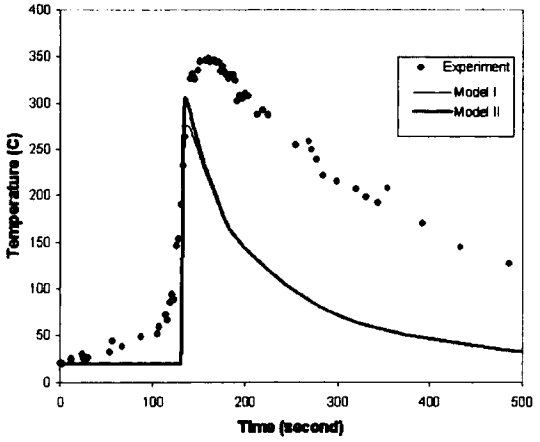

Fig. 7 Comparison of temperature profiles

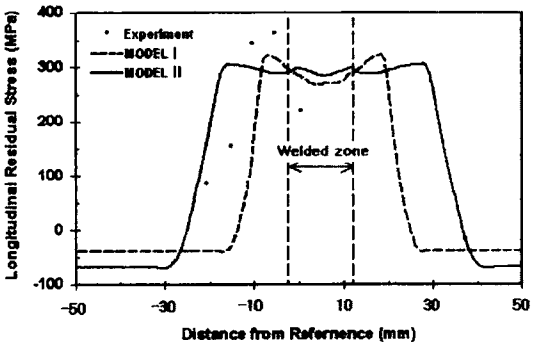

Fig. 8 Comparison of longitudinal residual stress distributions on the top surface of a five-pass welded plate

both magnitude and distribution demonstrate that the ramp-heating model is a viable alternative to the moving source model. Although both models underestimate the temperatures, the distribution gradients are very similar to the measured curve. Inaccurate description of welding heat input, inadequate boundary heat loss conditions, and other physical phenomena not considered in the numerical models have all contributed to the deviations.

Regardless of the inaccuracy of temperature predictions from different heat source models, as shown by the typical temperature representations at one location in the joint, it is of interest to assess the respective stress prediction capabilities and the significant characteristics of each temperature solution that could have the potential to predict reasonably accurate residual stress results with calibrations. The following section will address these issues.

4.2 Residual stress distributions

4.2.1 Longitudinal residual stress distribution

The predicted longitudinal residual stress distributions (along the welding direction) on the top surface for the two different heat source models and the experimental results obtained by the hole drilling method (HDM) in this study were compared in Fig. 8. The peak stress values for each heat input model were around 300 MPa; however, the experimental result showed 350 MPa. The width of the tensile zone for Model I and II were 38 and 61 mm, respectively. Showing this discrepancy between them in the width of the tensile residual stresses, it is due to the fact that the double ellipsoidal model has larger amount of heat input than the ramping heat source model as shown in Figs. 1 and 3. Both of the heat-source models predicted similar stress magnitude in the tensile zone. Figure 8 also shows the force equilibrium in the cross-section that leads to higher compressive stress in the base metal to counter balance the wider tensile zone.

4.2.2 Transverse residual stress distribution

Figure 9 shows a comparison between the predicted transverse residual stress distributions (perpendicular to the welding direction) obtained from the heat source models and the experimental results. The peak stress values predicted by Model I and II are 80 and 35 MPa, respectively. The combined widths of the predicted tensile and compressive zones from Models I and II are 40 and 60 mm, respectively. The trends of the predicted transverse residual stress distributions are much different from each other. In multi-pass welding, contraction of subsequent pass is always constrained by previous passes. The residual stresses generated from the earlier passes dominate the residual stresses of the final pass. The discrepancy of residual stresses along the plate thickness induces the compressive zone in

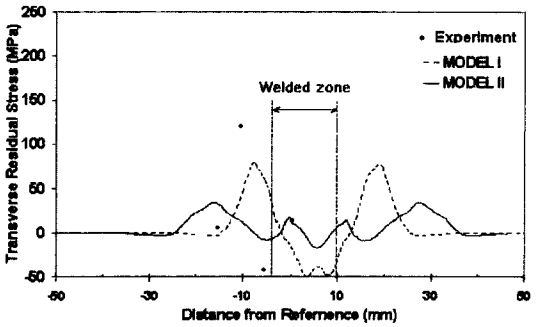

Fig. 9 Comparison of transverse residual stress distributions on the top surface of a five-pass welded plate

the weld metal and causes local bending of the plate. The peak transverse residual stresses predicted from Models I and II are located just a few millimeters away from the edge of the weld metal.

4.2.3 Characteristic temperature solution versus residual stress prediction

The temperature predictions using the FEA procedure often require incorporation of calibration coefficients, such as the heating fractions and the semi-axes of the ellipsoid in the moving source model, to fit the experimental data. These coefficients are purely empirical. In general, comparing the predicted peak temperature and the subsequent cooling with the experimental data provides sufficient information for evaluation of residual stresses.

The peak temperature region beyondmaterial's melting point represents an apparent shrinkage zone from a free-strain state to room temperature. This creates high-tensile residual stresses of yield magnitude in the region (i.e. weld metal). Peak temperatures greater than material's softening temperature range will generate high shrinkage plastic strains that eventually, upon cooling, lead to tensile residual stresses of yield magnitude in the region. On a contrary, the temperature gradients at temperatures lower than the material's softening temperature range will interact with the joint rigidity to form thermal strains that may or may not lead to shrinkage plastic strains. The total cumulative plastic strains, including all two contributions from different temperature regions, and their distributions result in the final state the residual stresses.

To assess the validity of a temperature solution for residual stress predictions, the peak temperature and the temperature gradient provide a proper base for estimating the residual stresses. Figure 7 shows a typical comparison of temperatures at a location in the joint. Although it shows deviations between different predictions and between predicted results and the measurement data, it seems that the predicted solutions from ramp heat model (Model I) and moving source model (Model II) share a common calibration constant when compared with the experiment temperature curve. Good fit with the measurement data could be accomplished by multiplying the predicted temperatures by the calibration constant. This would imply that characteristic shrinkage plastic strain distributions of reality might exist in the weldment when using the two heat source models. The calibration constant effect should be reflected in the magnitude of the predicted residual stress distributions.

Conclusions

This paper studied two most commonly used heat source models in the finite element analysis of welding-induced residual stresses. The double-ellipsoid moving heat source model is often referred in the studies and the ramping heat source model is often used for analysis of thick-section plate structures. Both models can predict characteristic temperature solutions for estimating residual stresses. Both models would also require calibrations to obtain accurate temperature results, but they can estimate reasonably accurate residual stresses without any temperature adjustments. This implies that the total cumulative shrinkage plastic strains at completion of welding could be calculated without using a detailed heat source model. This is due to the insensitivity of materials to high temperature details. The complex physical material behaviors at high temperature are after all become insignificant in contributing to the final formation of residual stresses.

Specific conclusions or observations derived from each thermo-mechanical analysis are summarized as follows:

(1) The temperature histories between heat source Models I and II are very similar to each other, but the width of tensile stress zone predicted using Model II is wider than that predicted by Model I. This indicates that the comparison of temperature histories is not sufficient to calibrate the finite element model.

(2) The magnitude of longitudinal residual stresses is insensitive to temperature histories. The magnitudes of the predicted longitudinal residual stresses, 300 MPa, are similar for both of the two models. And, the model type and the incorporated energy magnitude of the heat source affect to the width of the tensile stress zones of both longitudinal and transverse residual stresses.

(3) The double ellipsoidal heat input model predicted wider tensile stress zone then the ramp-heating model due to larger amount of heat input. The experimental data lay between the predicted models without compromising the prediction accuracy.

Acknowledgment

The authors are grateful for the support provided by a grant from the Korea Science and Engineering Foundation (KOSEF) and the Safety and Structural Integrity Research Center at the SungKyunKwan University.

References

ABAQUS User's Manual, 1998, Version 6.5

Argyris, J. H., Szimmat, J. and William, K. J., 1982, "Computational Aspects of Welding Stress Analysis," *Computer Methods in Applied Mechanics and Engineering*, Vol. 33, pp. 635~666.

Boulton and Lance Martin, 1936, "Residual Stresses in Arc-Welded Plates," *Proc. Institute of Mechanical Engineers*, Vol. 133, pp. 245~339.

Dong, Y., Hong, J. K., Tsai, C. L. and Dong, P., 1997, "Finite Element Modeling of Residual Stress in Austenitic Stainless Steel Pipe Girth Welds," *Welding Journal*, Vol. 76, No. 10, pp. 442~449.

Feng, Z., Jaeger, J., Kim, D. S., Lee, S., Papritan, J., Shim, Y. L. and Tsai, C. L., 1989, "Finite Element Modeling of Welded Thick Plates for Bonneville Navigation Lock," Research Report of Army Corps of Engineers.

Goldak, J., 1990, "Modeling Thermal Stresses and Distortion in Welds," Recent Trends in Welding Science and Technology, eds. S. A. David and I. M. Vitek, pp. 71~82.

Goldak, J., Chakravarti, A. and Bibby, M., 1984, "A New Finite Element Model for Welding Heat Sources," *Metallurgical Transactions B15B*, pp. 299~305.

Hibbitt, H. D. and Marcal, P. V., 1973, "A Numerical, Thermo-mechanical Model for the Welding and Subsequent Loading of a Fabricated Structure," *Computer & Structures*, Vol. 3, pp. 1145~1174.

Hong, J. K., 1996, "Study of Numerical Methodologies for Multi-Pass Welding Analysis," Ph. D. dissertation. Columbus, Ohio. The Ohio State University

Hong, J. K., Dong, P. and Tsai, C. L, 1994, "Finite element Simulation of Residual Stresses in Multi-pass Welds," International Conference Proceedings on Modeling and Control of Jointing Processes, ed. T. Zachria, American Welding Society, Miami, Fla., pp. 470~476.

Krutz, G. W. and Segerlind, 1978, *Welding Journal Research Supplement*, Vol. 57, pp. 211~216.

Lee, S. G., 1992, "Modeling of Residual Stress in Thick Section Weldments," Ph. D. Dissertation. Columbus, Ohio. The Ohio State University.

Leung, C. K. and Pick, R. J., 1990, "Finite Element Analysis of Multi-pass Welds," *Welding Research Council Bulletin*, Vol. 356, pp. 11~33.

Lindgren, L. E., 1986, "Temperature Fields in Simulation of Butt-welding of Large Plates," *Communications in Applied Numerical Methods*, Vol. 2, pp. 155~164.

Pavelic, V., Tanbakuchi, R., Uyehara, O. A. and Myers, P. S., 1969, "Experimental and Computed Temperature Histories in Gas Tungsten Arc Welding of Thin Plates," *Welding Journal*, Vol. 47, No. 7, pp. 295~305.

Seok, C. S., Suh, M. Y. and Park, J. H., 1999, "Investigation of Welding Residual Stress of High Tensile Steel by Finite Element Method and Experiment," *KSME International Journal*, Vol. 13, No. 12, pp. 879~885.

Shim, Y. L., Feng, Z., Lee, S. G., Kim, D. S., Jaeger, J. J., Papritan, J. C. and Tsai, C. L., 1992, "Determination of Residual Stresses in Thick-Section Weldment," *Welding Journal*, Vol. 71, No. 9, pp. 305~312.

Tsai, C. L., Kim, D. S., Shim, Y. L., Feng, Z., Lee, S., and Jaeger, J., 1991, "Determination of Residual Stress and Effects in Thick Section Weldments for Hydraulic Structures," Research Report of Army Corps of Engineers.

Tsai, C. L., Lee, S. G., Shim, Y. L., Jaeger, J. and Chasten, C., 1992, "Experimental Verification of Modeling Techniques of Thermal Related Welding Problems," *The Winter Annual Meeting of the ASME*, Orlando, Fla.

Ueda, Y. and Nakacho, K., 1982, "Simplifying Methods for Analysis of Transient and Residual Stresses and Deformations due to Multi-Pass Welding," *Trans. of JWRI*, Vol. 11, pp. 95~104.

Ueda, Y., Dakahashi, E., Fukuda, K., Sakamoto, K. and Nakacho, K., 1979, "Multi-pass Welding Stresses in Very Thick Plates and Their Reduction from Stress Relieve Annealing," *Trans. of JWRI*, Vol. 8, pp. 89~96.